Applied Physics Letters

Ohmic contact on low-doping-density p-type GaN with nitrogen-annealed Mg

Cite as: Appl. Phys. Lett. **119**, 242104 (2021); https://doi.org/10.1063/5.0076764
Submitted: 27 October 2021 • Accepted: 02 December 2021 • Published Online: 14 December 2021

Shun Lu, Manato Deki, Jia Wang, et al.

COLLECTIONS

EP This paper was selected as an Editor's Pick

View Online

Export Citation

CrossMark

ARTICLES YOU MAY BE INTERESTED IN

Vertical GaN p^+-n junction diode with ideal avalanche capability grown by halide vapor phase epitaxy
Applied Physics Letters **119**, 152102 (2021); https://doi.org/10.1063/5.0066139

GaN-based power devices: Physics, reliability, and perspectives
Journal of Applied Physics **130**, 181101 (2021); https://doi.org/10.1063/5.0061354

Vertical field inhomogeneity associated with threading dislocations in GaN high electron mobility transistor epitaxial stacks
Applied Physics Letters **119**, 243502 (2021); https://doi.org/10.1063/5.0066346

© 2021 Author(s).

Applied Physics Letters ARTICLE scitation.org/journal/apl

Ohmic contact on low-doping-density p-type GaN with nitrogen-annealed Mg

Cite as: Appl. Phys. Lett. **119**, 242104 (2021); doi: 10.1063/5.0076764
Submitted: 27 October 2021 · Accepted: 2 December 2021 ·
Published Online: 14 December 2021

Shun Lu,[1,a)] Manato Deki,[2] Jia Wang,[3] Kazuki Ohnishi,[1] Yuto Ando,[3] Takeru Kumabe,[1] Hirotaka Watanabe,[3] Shugo Nitta,[3] Yoshio Honda,[3] and Hiroshi Amano[2,3,4]

AFFILIATIONS

[1]Graduate School of Engineering, Nagoya University, Nagoya 464-8603, Japan
[2]Venture Business Laboratory, Nagoya University, Nagoya 464-8603, Japan
[3]Institute of Materials and Systems for Sustainability, Nagoya University, Nagoya 464-8601, Japan
[4]Akasaki Research Center, Nagoya University, Nagoya 464-8603, Japan

[a)]Author to whom correspondence should be addressed: lu.shun@c.mbox.nagoya-u.ac.jp

ABSTRACT

We have demonstrated a fabrication process for the Ohmic contact on low-doping-density p-type GaN with nitrogen-annealed Mg. An Ohmic contact with a contact resistance of $0.158\,\Omega\ \text{cm}^2$ is realized on p^--GaN ([Mg] $= 1.3 \times 10^{17}\ \text{cm}^{-3}$). The contact resistance of p-type GaN with higher Mg concentration ([Mg]$=1.0 \times 10^{19}\ \text{cm}^{-3}$) can also be reduced to $2.8 \times 10^{-5}\,\Omega\ \text{cm}^2$. A localized contact layer is realized without any etching or regrowth damage. The mechanism underlying this reduced contact resistance is studied by scanning transmission electron microscopy with energy dispersive x-ray spectroscopy and secondary ion mass spectrometry, representing a mutual diffusion of Ga and Mg atoms on the interface. Reductions in the barrier height and surface depletion width with the nitrogen-annealed Mg layer are confirmed by XPS and Hall effect measurements qualitatively.

Published under an exclusive license by AIP Publishing. https://doi.org/10.1063/5.0076764

Gallium nitride (GaN) is a potential semiconductor material in power device fields because of its high breakdown electrical field, high saturated electron velocity, and high electron mobility.[1] To realize various GaN power devices, such as metal-oxide-semiconductor field-effect transistors (MOSFETs) or heterojunction bipolar transistors (HBTs),[1–6,33] the formation of a low-resistance Ohmic contact between GaN and an electrode metal is important.[7,8] For the n-type GaN Ohmic contact, a Ti/Al electrode can easily achieve a low-resistance Ohmic contact below $1.0 \times 10^{-5}\,\Omega\ \text{cm}^2$.[8–10] On the other hand, the p-GaN Ohmic contact still remains a problem. Because of the depletion mode of band bending, the contact between p-type GaN and a metal is always a Schottky contact with high resistance. The most popular Ni/Au electrode with post-metallization annealing in oxygen ambient can reduce the contact resistance because of p-type NiO formation.[11–13] A specific contact resistance below $1.0 \times 10^{-4}\,\Omega\ \text{cm}^2$ was reported to be obtained on p-type GaN with a hole concentration of $10^{17}\ \text{cm}^{-3}$. However, the technique of fabricating such a contact still relies on the tunneling effect through a thinned barrier and is restricted to high-doping-density p^+-GaN. Direct Ohmic contact on low-doping-density p-type GaN is still difficult to realize and has caused many problems. Regarding p-GaN electrical property assessment, Hall effect measurements on p-GaN with low Mg concentrations are difficult because of the Schottky contact. In the practical power device processes, such as that for vertical GaN MOSFETs, body contact between p-GaN and a source electrode is necessary to stabilize the threshold voltage.[6] In other device structures such as GaN HBTs, p-type Ohmic contact problems at base contacts also need to be addressed.[5] In GaN p-FETs, which are important parts of GaN integrated circuits, the contact resistance between the source/drain electrode and p-GaN should also be reduced to realize a higher on-current density.[3,14,15] One way of reducing the contact resistance on low-doping-density p-GaN is by forming a thin p^+ contact layer between the electrode and p-GaN.[16] Continuous growth of a thin p^+ contact layer during metal-organic vapor phase epitaxy (MOVPE) crystal growth is the most common approach. However, a full surface contact layer formed in this way requires dry etching after growth and may introduce plasma-induced damage to the surface.[17,18] Other methods, such as selective area regrowth, may also lead to a contamination layer on the interface and affect the device property.[19,20] Ion implantation or diffusion is also difficult because high temperature and high pressure are required. All these problems make Ohmic contact formation on low-doping-density p-type GaN a bottleneck of the GaN power device process.

Published under an exclusive license by AIP Publishing

In this work, to solve the p-type Ohmic contact problem, we introduced another p-type contact layer process by using nitrogen-annealed Mg. p-GaN with low Mg concentrations ($[Mg] = 1.3 \times 10^{17}\ cm^{-3}$) grown by MOVPE shows the Ohmic contact with the contact layer. The specific contact resistance determined by circle transmission line measurement (CTLM) was $0.158\ \Omega\ cm^2$. The contact resistance of p-GaN with a higher Mg concentration ($[Mg] = 1.0 \times 10^{19}\ cm^{-3}$) by the same process can also be reduced to $2.8 \times 10^{-5}\ \Omega\ cm^2$, which is comparable to those of samples with the continuous growth of the p^+ layer. Compared with conventional methods, the entire process requires a lower temperature and a simpler operation. A contact layer localized on a specific region is also easily obtained by photolithography while depositing Mg, free of any etching- or regrowth-induced damage.

Figure 1 shows schematic illustrations of CTLM samples. To measure the extent of contact resistance improvement of our contact layer, two types of the p-GaN sample with different Mg concentrations were grown by MOVPE. During the growth of sample (a), a 30 nm low-temperature GaN buffer layer/3.5 μm u-GaN/300 nm n^+-GaN ([Si]: $1.3 \times 10^{18}\ cm^{-3}$)/3 μm n-GaN ($[Si] = 2 \times 10^{16}\ cm^{-3}$) was first grown on a sapphire substrate. Then, 1.3 μm p-GaN ($[Mg] = 1.3 \times 10^{17}\ cm^{-3}$) was grown. Sample (b) was grown on a GaN substrate ($[Si] = 1 \times 10^{18}\ cm^{-3}$). A 1 μm n-GaN layer ($[Si] = 2 \times 10^{16}\ cm^{-3}$) was first grown. Then, 2 μm p-GaN ($[Mg] = 1 \times 10^{19}\ cm^{-3}$) was grown. There was no p^+ layer on either of the two samples. The Mg concentration was measured by secondary ion mass spectrometry (SIMS). The thickness of the p-GaN layer in both structures was sufficient for CTLM measurement. The samples were first cleaned in sulfuric peroxide mix (SPM, H_2SO_4:H_2O_2 = 1:1), diluted HF (DHF, HF:H_2O = 1:9), standard clean-1 (SC1, NH_4OH:H_2O_2:H_2O = 1:1:5), and standard clean-2 (SC2, HCl:H_2O_2:H_2O = 1:1:6) with rinsing in de-ionized water after each cleaning step to remove surface oxides, metal ions, and particle contamination.[21] After cleaning, they were annealed in 700 °C N_2 ambient for 5 min for Mg activation.[22] Mg was deposited by radio frequency magnetron sputter and then patterned to the CTLM electrode configuration after liftoff. The thickness of Mg is 50 nm as confirmed using a step profiler. The samples with Mg were then put into a rapid thermal annealing (RTA) system and annealed in N_2 ambient at 800 °C for 60 min. After annealing, they were washed in boiled *aqua regia* and diluted HF for 15 min each. The Mg deposition, N_2 annealing, and post-annealing acid washing were carried out to form the annealed Mg layer, which are the key points of this study. After the formation of the annealed Mg layer, a 20/150-nm-thick CTLM patterned Ni/Au electrode was then deposited on the contact layer with an electron beam (EB) evaporator. There was a 2 μm margin for any misalignment between the Ni/Au electrode and the annealed Mg layer. Finally, the samples were annealed in 525 °C O_2 ambient for 5 min. The current–voltage characteristics of the CTLM sample were measured at various gap lengths. The dimensions and gap lengths of the CTLM samples are shown in Fig. 1(c).

The Mg thickness and other parameters were changed to determine the best process condition. The structure of the annealed Mg contact layer was then studied by scanning transmission electron microscopy (STEM) with energy dispersive x-ray (EDX) spectroscopy. The sample for STEM was prepared by the same method without HF and *aqua regia* washing. SIMS was performed on samples after acid washing to measure the Mg concentration in p-GaN. Finally, surface band bending of the samples with and without an annealed Mg layer was measured by both XPS and Hall effect measurement to confirm their surface electrical properties. All the experiments for studying the parameters and mechanism underlying the contact resistance were carried out on sample (a), which had a lower Mg concentration of $1.3 \times 10^{17}\ cm^{-3}$.

Figure 2(a) shows the typical current–voltage characteristics of both samples with and without an annealed Mg layer. The contact between the Ni/Au electrode and p-GaN with a Mg concentration of

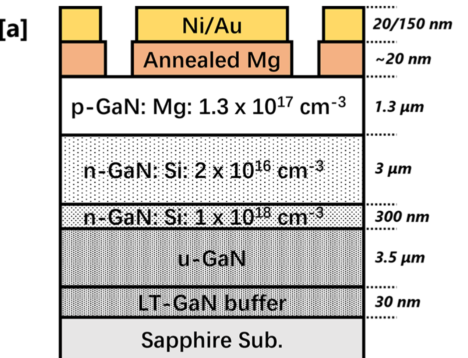

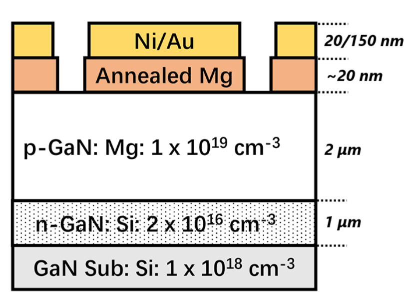

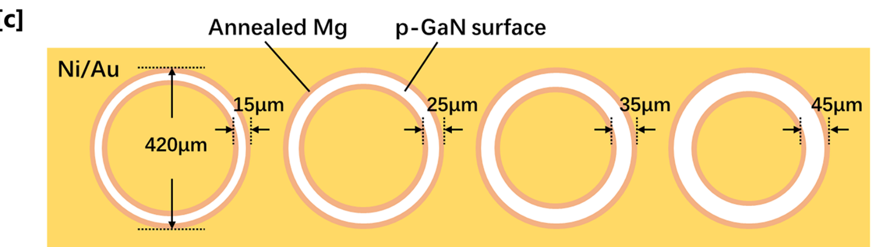

FIG. 1. Sample structures for CTLM of (a) low- and (b) high-Mg-concentration p-GaN with annealed Mg layer. (c) Top view of CTLM samples with gap width and electrode dimensions of the CTLM pattern. The margin for the misalignment between Ni/Au and annealed Mg is 2 μm.

Published under an exclusive license by AIP Publishing

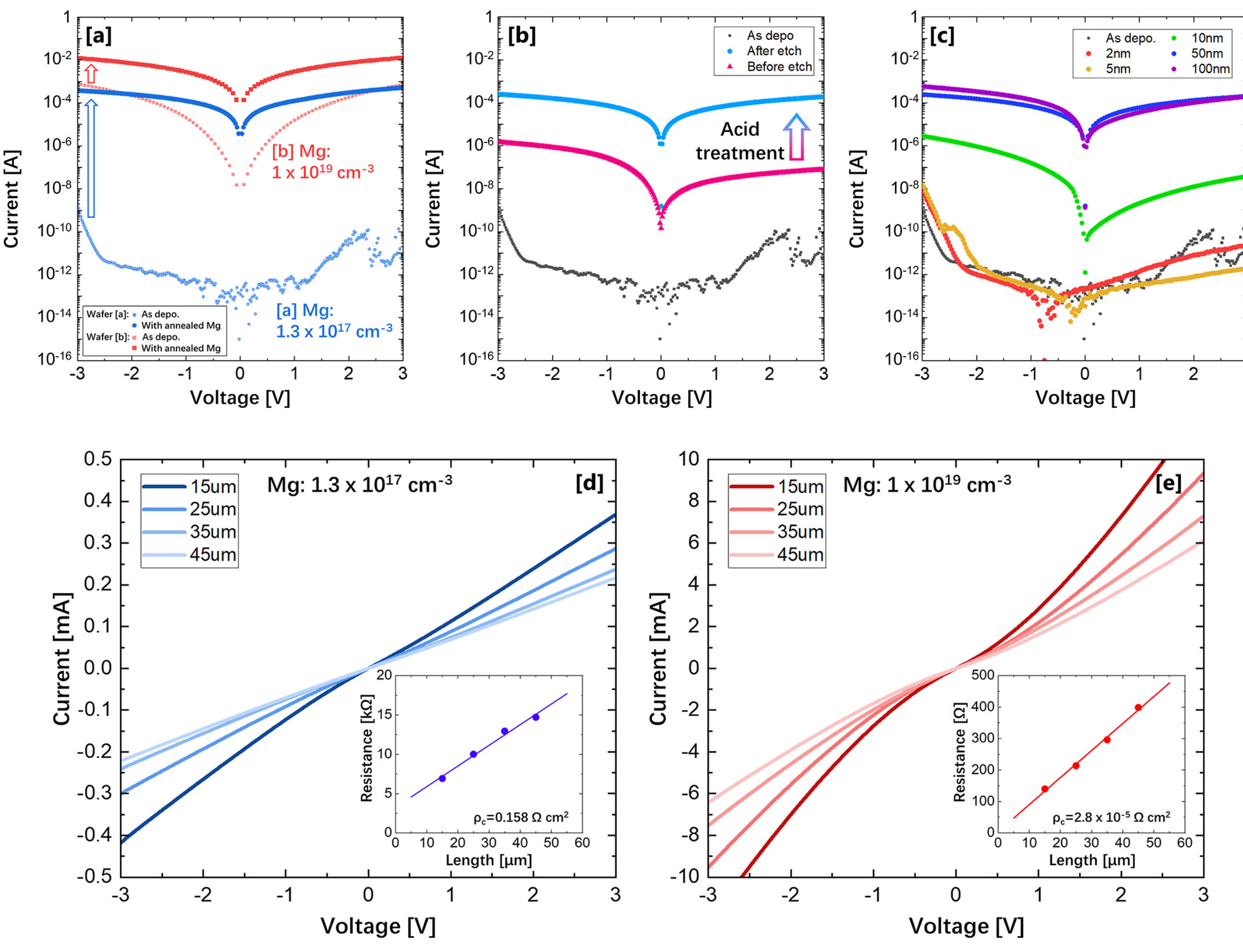

FIG. 2. (a) Typical current–voltage characteristics with and without the annealed Mg layer. (b) Effect of *aqua regia*/HF treatment after annealing. (c) Current–voltage characteristics influenced by the thickness of Mg deposited by sputtering before annealing. Current–voltage and resistance-distance dependence on p-GaN with (d) low and (e) high Mg concentrations as determined by CTLM.

$1.3 \times 10^{17}\,\text{cm}^{-3}$ is almost insulating because of the high barrier. The contact resistance could not be determined because of the low current and current–voltage nonlinearity. By forming an annealed Mg contact layer, the current increases about 10^5 times. For sample (b) with a Mg concentration of $1 \times 10^{19}\,\text{cm}^{-3}$, the current also increases with the annealed Mg layer especially when the voltage is low. After annealing in nitrogen, the Mg layer became thicker (∼80 nm) and lost surface metal luster. A rough brown layer was formed. After washing, about 20–40 nm of the layer was left. The root mean square surface roughness was 10.4 nm as determined by AFM ($5 \times 5\,\mu$m), which is much larger than that of the original p-GaN wafer. The effect of washing in HF and *aqua regia* is also proved by the current–voltage relation shown in Fig. 2(b). Before HF/*aqua regia* treatment, the increase in current is limited, and the linearity is insufficient. A possible fixed-value resistor is formed between the Ni/Au electrode and p-GaN. The decrease in thickness (before washing: ∼80 nm; after washing: 20–40 nm) also suggests that part of the layer was removed after washing in HF/*aqua regia*. On the other hand, the remaining 20–40 nm annealed Mg layer cannot be removed even with long-time acid washing and is, thus, considered nonreactive with acid. We found that 15 min is sufficient for removing the entire resistor-like layer. The thickness dependence of Mg deposited by the sputtering system before annealing was also studied on sample (a) as shown in Fig. 2(c). The figure shows that the current increases and the linearity improves when a thicker Mg layer is deposited and there is a maximum improvement at 50 nm. Also, a very thin Mg layer leads to little improvement in the contact. This may be due to the oxidation of the Mg layer as the samples were exposed to air as they were transported from the sputtering system to RTA after Mg deposition. Other Mg deposition methods, such as the EB evaporator, were also used, and the current–voltage results were almost the same.

CTLM results in Figs. 2(d) and 2(e) show that the current–voltage characteristics are close to linear, showing that good Ohmic contact is obtained on both samples. The current increase and linearity improvement, especially on sample (a) with a low Mg concentration of $1.3 \times 10^{17}\,\text{cm}^{-3}$, in which the Ohmic contact is generally considered difficult to achieve, prove the effectiveness of the nitrogen-annealed Mg contact layer. The insets in Figs. 2(d) and 2(e) show the

Published under an exclusive license by AIP Publishing

distance dependence of the resistance between the electrodes. The specific contact resistance is calculated from the fit of the resistance-length relationship with the CTLM correction factor.[23] On the basis of the linear fit, a specific Ohmic contact resistance of 0.158 Ω cm^2 at V = −2.5 V is reached on p-GaN with Mg concentration 1.3×10^{17} cm^{-3}. The contact resistance of p-GaN with a Mg concentration of 1×10^{19} cm^{-3} can also be reduced from 1.2×10^{-2} Ω cm^2 (distance dependence not shown here) to 2.8×10^{-5} Ω cm^2 at V = −5 V. The current–voltage results of both the low- and high-Mg-concentration p-GaN prove the potential of nitrogen-annealed Mg as a solution to the problems of the p-type Ohmic contact. Also, the process does not include dry etching, which can introduce plasma-induced damage, and the annealed Mg layer can be easily localized by photolithography.

Figures 3(a)–3(d) show the STEM EDX images of the layered structure in the nitrogen-annealed Mg layer on sample (a) without post-annealing washing in acid. From the Mg and O signals, the top of the annealed Mg layer is amorphous MgO-like. It is considered to be formed after Mg deposition by sputtering and before annealing. The surface of the Mg layer reacts with oxygen and H_2O in air,[24] forming $MgO/Mg(OH)_2$ on the top. (H signal was not measured here.) This oxide-like layer may have been removed during post-annealing washing in HF and Aqua regia, which explains the improvement of the current–voltage characteristics after washing as shown in Fig. 2(b).

Below the MgO-like layer is a layer with Mg, Ga, N, and weak O signal. It is considered a mixture of $(Mg_3N_2)_{1-x}(GaN)_x$, which is called MgGaN here. In Fig. 3(c), the crystallinity of the MgGaN layer is discontinuous in comparison with that of p-GaN below. XRD was performed on the surface, which showed no obvious crystalline pattern (XRD figure not shown here) that is considered to form during annealing such as Mg_3N_2.[25] From the EDX images, the GaN surface decomposes, and Ga diffuses outward. The activation among Ga, Mg, and N (from both GaN and N_2) then leads to the formation of the MgGaN layer. The Ga signal strength difference between the MgGaN layer and the original p-GaN shows the GaN decomposition and outward movement of Ga [Fig. 3(d), Ga signal]. With this critical Ga

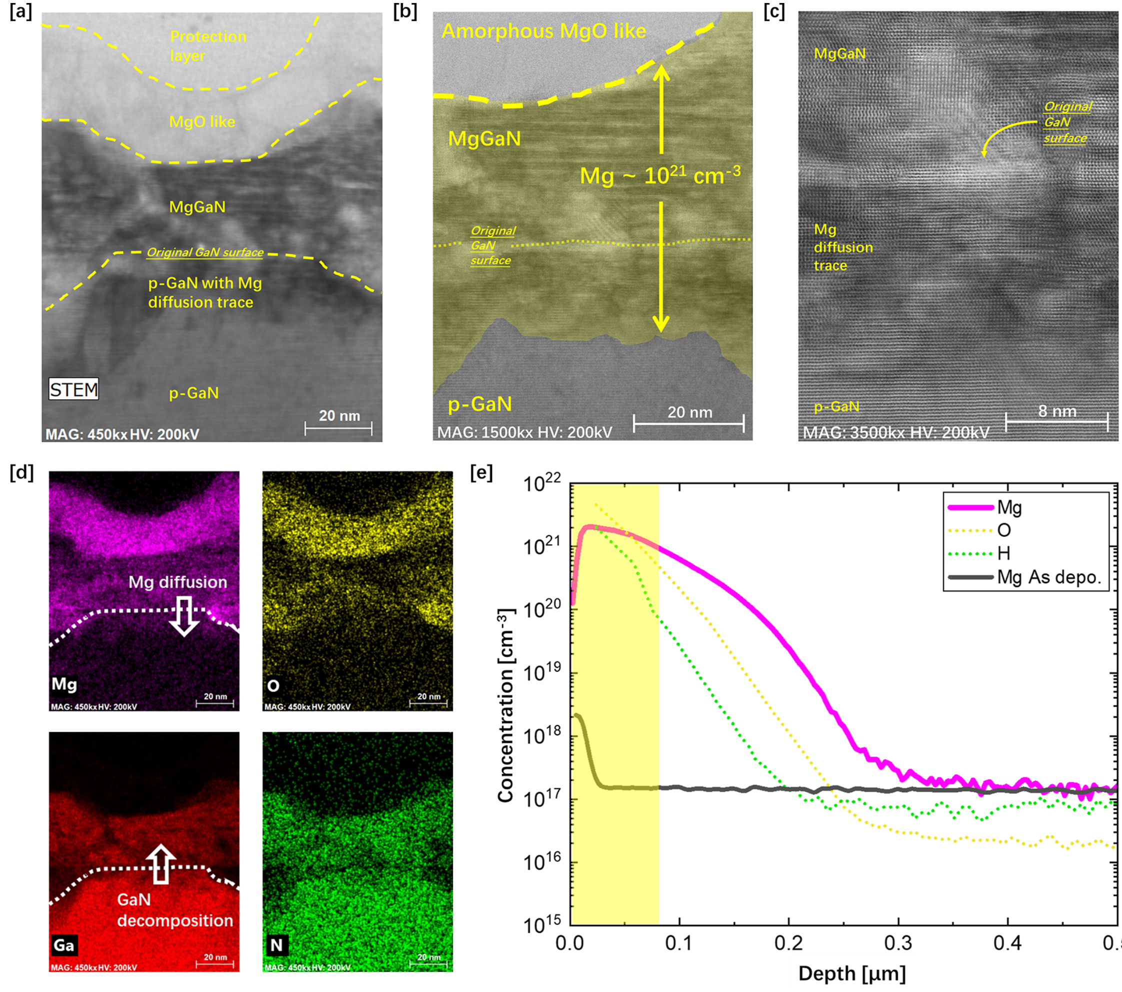

FIG. 3. (a)–(c) STEM images at different magnifications of the annealed Mg/GaN interface before washing; (d) EDX-measured Mg/Ga/O/N signals in the background of (a); (e) concentrations of Mg and other impurities measured by SIMS compared with the signal of Mg in (b).

Published under an exclusive license by AIP Publishing

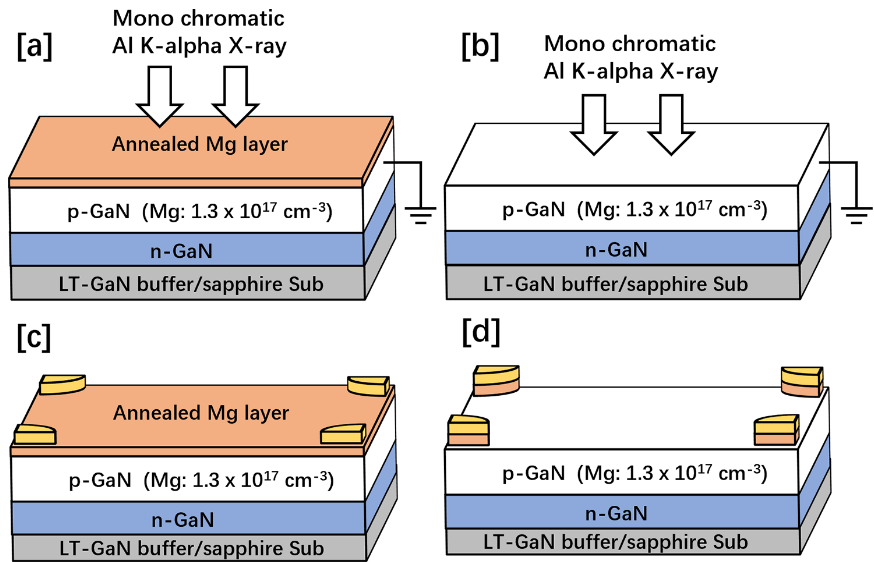

FIG. 4. Sample structures of XPS and Hall effect measurements. (a) and (c) Samples with nitrogen-annealed Mg layer covering the entire surface; (b) and (d) Samples without annealed Mg layer or with partially patterned layer under the electrodes.

atom outward movement, Ga vacancies remain in p-GaN, and Mg diffuses inside easily. The Mg diffusion trace in the original p-GaN can also be observed in the STEM figure. Previous results on the Mg diffusion on p-GaN with powder Mg_3N_2 show similar contact improvement, and the mechanism of which is considered similar to that of this work.[26] The thickness change mentioned above suggests that the MgGaN layer is the layer remaining after washing in *aqua regia* and HF. This type of mutual diffusion between Ga and Mg atoms and MgGaN formation also stabilize the layer, because without Ga, the Mg_3N_2 thin film is very unstable in air.[25,27] We tried the same process on sapphire and Si substrates, and there was almost no layer left on non-GaN substrates after annealing because of the Mg_3N_2 hydrolyzation.

The concentrations of Mg and other impurities in p-GaN with the annealed Mg layer after acid treatment were measured by SIMS and shown in Fig. 3(e). The Mg diffusion depth is about 250 nm with the average Mg concentration of about $1 \times 10^{19}\,cm^{-3}$. The same region with a high Mg concentration is highlighted in the STEM image in Fig. 3(b) and the SIMS profile in Fig. 3(e) for comparison. In comparison with the former Mg diffusion results,[28] our process requires a lower temperature and can achieve a higher Mg concentration, owing to the introduction of Ga vacancies into the original p-GaN. However, in our study, because of the direct deposition of Mg on the GaN surface, the Mg concentration is extremely high especially in the remaining MgGaN layer, much higher than the Mg concentration in p-GaN. This means that the top high-Mg-concentration layer may lead to impurity tails in the SIMS profile and disturb the later measurement of the Mg concentration in p-GaN.[29] The roughness of the annealed Mg surface may also seriously affect the measurement of the Mg concentration as well as the surface element composition, similarly to the previous results on Si and GaAs.[30,31] In Fig. 3(e), there is an unusual signal of Mg on the surface (10 nm) of the sample, which is considered to be due to the rough surface of MgGaN. Moreover, considering the fact that part of the N atoms in the original p-GaN may also diffuse outward and bond with Mg because of GaN decomposition, it is also easier for O and other impurities that can fit in N vacancies to diffuse inside and passivate Mg. Impurities in the sputtering Mg target and the vacuum discontinuity of the entire process may be the sources of these impurities. The concentrations of O and H were also measured by SIMS and shown in Fig. 3(e). Nevertheless, the SIMS results still qualitatively confirm the Mg diffusion in p-GaN and a possible p^+ layer formation, which may explain the contact resistance reduction.

To confirm the surface electrical properties after the nitrogen-annealed Mg process, the surface barrier height and depletion length of sample (a) before and after the process were measured by XPS and room-temperature Hall effect measurements. In the XPS measurement, the bulk Fermi level was fixed with carbon tape so that the surface valence band maximum (VBM) can be measured [Figs. 4(a) and 4(b)]. In room-temperature Hall effect measurement, the sheet resistance and sheet hole concentration of the samples with the annealed Mg layer covering the entire sample surface and partially patterned on the sample surface under the Ni/Au electrode were measured [Figs. 4(c) and 4(d)]. Data on the VBM determined by XPS measurement and sheet resistance, hole mobility, and sheet hole concentration

TABLE I. VBM, sheet resistance, hole mobility, and sheet hole concentration.

Structure	Valence band maximum (eV)	Sheet resistance (Ω/□)	Hole mobility (cm^2/V s)	Sheet hole concentration (cm^{-2})
As depo. p-GaN [Fig. 4(d)]	3.2	1.73×10^5	23.2	1.56×10^{12}
Annealed Mg/p-GaN [Fig. 4(c)]	1.1	1.55×10^5	22.5	1.79×10^{12}

Published under an exclusive license by AIP Publishing

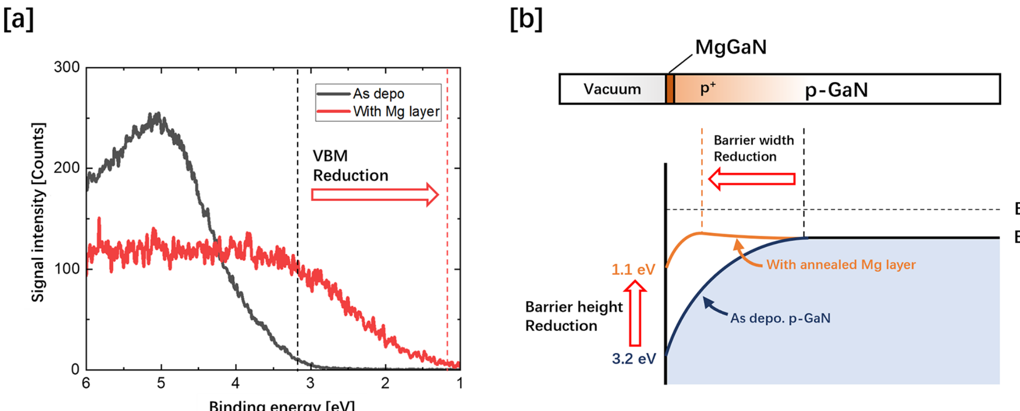

FIG. 5. (a) VBM reduction determined by XPS measurement. (b) Surface band structure of as depo. p-GaN (dark blue line) and p-GaN with annealed Mg layer (brown line).

determined by Hall effect measurement are listed in Table I for comparison. In Fig. 5(a), the VBM decrease leads to the reduction in the barrier height after the process. The VBM reduction is also confirmed on sample (b) with a higher Mg concentration, proving the relaxation of surface band bending with the annealed Mg layer. During Hall effect measurement, with a similar hole mobility (within an error range of 3%), the sheet resistance decreased whereas the sheet hole concentration increases about 15% when the annealed Mg layer covers the entire sample surface. It shows a larger effective thickness of p-GaN in the Hall effect measurement and a smaller surface depletion width. The effective thickness of p-GaN in Figs. 4(a) and 4(b) was calculated using the barrier height measured by XPS, and its variation fits well with the increase in the sheet hole concentration determined by Hall effect measurement in Figs. 4(c) and 4(d). Also, the structure shown in Fig. 4(d) and its result in Table I show the practical applicability of the annealed Mg contact layer in the low-Mg-concentration p-GaN Hall effect measurement. The results of XPS and Hall effect measurement suggest that the MgGaN layer may change the energetic position of the surface Fermi level pinning,[32] which is another possible explanation for the contact resistance reduction. These results of the surface electrical property also suggest that this Mg annealing process is not just a conventional diffusion but a combination of Mg diffusion and surface state variations. By taking together the VBM reduction determined by XPS, Hall effect measurement results, and the possible Mg diffusion proved by STEM EDX and SIMS, we show in Fig. 5(b) the valence band structure with and without the annealed Mg layer with a lower barrier and a smaller depletion width. The change in the surface band structure explains the reduction in the contact resistance.

In this work, we obtained a localized Ohmic contact on p-GaN with a Mg concentration of $1.3 \times 10^{17}\,\mathrm{cm}^{-3}$ with a nitrogen-annealed Mg layer. An Ohmic contact with a contact resistance of $0.158\,\Omega\,\mathrm{cm}^2$ was realized. The contact resistance of p-GaN with a higher Mg concentration of $1.0 \times 10^{19}\,\mathrm{cm}^{-3}$ was also reduced to below $10^{-4}\ \Omega\,\mathrm{cm}^2$ with the same process. STEM EDX and SIMS were performed on the sample to clarify the internal structure of the contact layer. The mutual diffusion of Ga and Mg atoms and the formation of MgGaN were observed. XPS and Hall effect measurement results show band bending relaxation after the process. Compared with other conventional methods such as continuous growing or regrowth, our process requires a lower temperature and pressure and can achieve a localized contact layer easily without any etching-induced damage.[33] We consider that it is a practical solution to overcoming the p-GaN Ohmic contact bottleneck.

This work was supported by the MEXT-Program for Creation of Innovative Core Technology for Power Electronics via Grant No. JPJ009777.

AUTHOR DECLARATIONS

Conflict of Interest

The authors have no conflicts to disclose.

DATA AVAILABILITY

The data that support the findings of this study are available from the corresponding author upon reasonable request.

REFERENCES

[1]H. Amano, Y. Baines, E. Beam, M. Borga, T. Bouchet, R. Chu, C. D. Santi *et al.*, J. Phys. D: Appl. Phys. **51**, 163001 (2018).
[2]S. T. Sheppard, K. Doverspike, W. L. Pribble, S. T. Allen, J. W. Palmour, L. T. Kehias, and T. J. Jenkins, IEEE Electron Device Lett. **20**, 161 (1999).
[3]Z. Zheng, L. Zhang, W. Song, S. Feng, H. Xu, J. Sun, S. Yang, T. Chen, J. Wei, and K. J. Chen, Nat. Electron. **4**, 595 (2021).
[4]S. Kawasaki, Y. Ando, M. Deki, H. Watanabe, A. Tanaka, S. Nitta, Y. Honda, M. Arai, and H. Amano, Appl. Phys. Express **14**, 046501 (2021).
[5]H. Xing, P. M. Chavarkar, S. Keller, S. P. DenBaars, and U. K. Mishra, IEEE Electron Device Lett. **24**, 141 (2003).
[6]W. Li, K. Nomoto, K. Lee, S. M. Islam, Z. Hu, M. Zhu, X. Gao, M. Pilla, D. Jena, and H. G. Xing, IEEE Trans. Electron Devices **65**, 2558 (2018).
[7]Q. Z. Liu and S. S. Lau, Solid State Electron **42**, 677 (1998).
[8]G. Greco, F. Iucolano, and F. Roccaforte, Appl. Surf. Sci. **383**, 324 (2016).
[9]B. P. Luther, S. E. Mohney, T. N. Jackson, M. Asif Khan, Q. Chen, and J. W. Yang, Appl. Phys. Lett. **70**, 57 (1997).
[10]B. Van Daele, G. Van Tendeloo, W. Ruythooren, J. Derluyn, M. R. Leys, and M. Germain, Appl. Phys. Lett. **87**, 061905 (2005).
[11]J. K. Sheu, Y.-K. Su, G.-C. Chi, P. L. Koh, M. J. Jou, C. M. Chang, C. C. Liu, and W. C. Hung, Appl. Phys. Lett. **74**, 2340 (1999).
[12]D. Qiao, L. S. Yu, S. S. Lau, J. Y. Lin, H. X. Jiang, and T. E. Haynes, J. Appl. Phys. **88**, 4196 (2000).

Published under an exclusive license by AIP Publishing

[13]J.-K. Ho, C.-S. Jong, C. C. Chiu, C.-N. Huang, C.-Y. Chen, and K.-K. Shih, Appl. Phys. Lett. **74**, 1275 (1999).
[14]N. Chowdhury, J. Lemettinen, Q. Xie, Y. Zhang, N. S. Rajput, P. Xiang, K. Cheng, S. Suihkonen, H. W. Then, and T. Palacios, IEEE Electron Device Lett. **40**, 1036 (2019).
[15]N. Chowdhury, Q. Xie, M. Yuan, N. S. Rajput, P. Xiang, K. Cheng, H. W. Then, and T. Palacios, in *IEEE International Electron Devices Meeting* (IEEE, 2019), pp. 4.6.1–4.6.4.
[16]F. Liang, D. Zhao, D. Jiang, Z. Liu, J. Zhu, P. Chen, J. Yang, W. Liu, X. Li, S. Liu, Y. Xing, L. Zhang, H. Yang, H. Long, and M. Li, J. Cryst. Growth **467**, 1–5 (2017).
[17]X. A. Cao, S. J. Pearton, A. P. Zhang, G. T. Dang, F. Ren, R. J. Shul, L. Zhang, R. Hickman, and J. M. Van Hove, Appl. Phys. Lett. **75**, 2569 (1999).
[18]T. Kumabe, Y. Ando, H. Watanabe, M. Deki, A. Tanaka, S. Nitta, Y. Honda, and H. Amano, Jpn. J. Appl. Phys., Part 1 **60**, SBBD03 (2021).
[19]K. Fu, H. Fu, H. Liu, S. R. Alugubelli, T.-H. Yang, X. Huang, H. Chen, I. Baranowski, J. Montes, and F. A. Ponce, Appl. Phys. Lett. **113**, 233502 (2018).
[20]K. Fu, H. Fu, X. Deng, P. Y. Su, H. Liu, K. Hatch, C. Y. Cheng, D. Messina, R. V. Meidanshahi, P. Peri, C. Yang, T. H. Yang, J. Montes, J. Zhou, X. Qi, S. M. Goodnick, F. A. Ponce, D. J. Smith, R. Nemanich, and Y. Zhao, Appl. Phys. Lett. **118**, 222104 (2021).
[21]S. W. King, J. P. Barnak, M. D. Bremser, K. M. Tracy, C. Ronning, R. F. Davis, and R. J. Nemanich, J. Appl. Phys. **84**, 5248 (1998).
[22]S. Nakamura, T. Mukai, M. Senoh, and N. Iwasa, Jpn. J. Appl. Phys., Part II **31**, L139 (1992).
[23]D. K. Schroder, *Semiconductor Material and Device Characterization* (IEEE, 2006), pp. 127–184.
[24]S. Ogawa, H. Niwa, K. Nakanishi, T. Ohta, and S. Yagi, J. Surf. Anal. **17**, 319 (2011).
[25]S. Wang, X. Chen, X. Liu, Z. Chen, X. Liu, J. Zhao, L. Qiu, L. Hou, and Y. Gao, Thin Solid Films **711**, 138271 (2020).
[26]C. C. Chen, J. L. Yen, and Y. J. Yang, in *Conference on Lasers and Electro-Optics* (Optical Society of America, 2001), p. CTuW6.
[27]P. John, P. Vennéguès, H. Rotella, C. Deparis, C. Lichtensteiger, and J. Zúñiga-Pérez, J. Appl. Phys. **129**, 095303 (2021).
[28]C. J. Pan and G. C. Chi, Solid-State Electron. **43**, 621 (1999).
[29]M. A. Reshchikov, M. Vorobiov, O. Andrieiev, K. Ding, N. Izyumskaya, V. Avrutin, A. Usikov, H. Helava, and Y. Makarov, Sci. Rep. **10**, 2223 (2020).
[30]S. B. Herner, J. Vac. Sci. Technol. B **14**, 3593 (1996).
[31]M. Rei Vilar, J. El Beghdadi, F. Debontridder, R. Artzi, R. Naaman, A. M. Ferraria, and A. M. Botelho do Rego, Surf. Interface Anal. **37**, 673 (2005).
[32]T. Hashizume, J. Appl. Phys. **94**, 431 (2003).
[33]J. Wang, S. Lu, W. Cai, T. Kumabe, Y. Ando, Y. Liao, Y. Honda, Y.-H. Xie, and H. Amano, IEEE Electron Device Letters **43**, 1 (2022).

Published under an exclusive license by AIP Publishing